Thermal performance of starch/beet-pulp composite bricks for building insulation at a wall scale

Elias Harb, Chadi Maalouf, Christophe Bliard, Martin Tenpierik, Mohammed Lachi, Fabien Bogard, Guillaume Polidori

Thermal Performance of Starch/Beet-pulp Composite Bricks for Building Insulation at a Wall Scale

Elias Harb[1], Chadi Maalouf[1], Christophe Bliard[2], Martin Tenpierik[3], Mohammed Lachi[1], Fabien Bogard[1,4], Guillaume Polidori[1]

[1]Laboratoire de MATériaux et Ingénieurie Mécanique, MATIM, Université de Reims-Champagne-Ardenne URCA, Moulin de la Housse, 51687 Reims Cedex 2, France

[2]Institut de Chimie Moléculaire de Reims, ICMR-UMR 7312 CNRS, Université de Reims-Champagne-Ardenne URCA, Moulin de la Housse, 51687 Reims Cedex 2, France

[3] Department of Architectural Engineering and Technology, Faculty of Architecture and the Built Environment, Delft University of Technology, Julianalaan 134, 2628BL Delft, the Netherlands

[4] Pôle de Recherche Châlonnais, Université de Reims Champagne Ardenne, Châlons en Champagne, France

Abstract

This paper aims to study the thermal performance at wall scale of hollowed bricks made of starch/beet-pulp bio-composites identified as a potent solution for the development of sustainable, non-load bearing, insulation materials to be used in the construction sector. Numerical studies on thermal resistance using the COMSOL software were conducted to study the characteristics of optimal hollowed brick pattern. The numerical study results were then compared with thermal resistance calculations based on the NF EN ISO norm 6946 (2017). In a later stage, an experimental 1m x 1m wall made of starch/beet-pulp composite bricks and binder was built. Experimental studies on the thermal resistance and thermal imaging were carried out on the wall inserted in a bi-climatic chamber showing only a 3°C change of the surface temperature of the wall on the one side after applying a 23°C temperature difference on the other side for 7h. The equivalent thermal resistances were obtained equal to 1.180 m^2.K/W, 1.218 m^2.K/W, 1.10 m^2.K/W respectively as described previously which reflected a good agreement between the numerical and experimental results.

Finally, the obtained results reflected the high thermal performance of the studied starch/beet-pulp composites.

Keywords: beet-pulp, starch, hollowed brick, thermal performance, COMSOL Multiphysic 2D*, NF EN ISO norm 6946 (2017), thermal imaging* bi-climatic chamber.

I. Introduction

Global warming coupled with continuous increase in building energy consumption has set off the international alarm. Over and above that, an additional growth by about 40% in building energy usage is estimated to occur in the next 20 years due to increasing demand for thermal comfort (Mariano-Hernández et al.) Therefore, the adoption of sustainable, energy saving and eco-friendly technologies in the building sector based on low cost bio-based materials has become an emergency response plan worldwide. Subsequently 75,000 tons of fossil fuels are likely to be saved in France in 2050 while avoiding the rejection of 312,771 tCO2eq due to an energy recovery from bio-based insulation wastes (Rabbat et al.2022).

The continuous population and economy growth has led to an exponential increase in global energy demand with more than 80% of the current primary energy consumed is produced from fossil fuels that is likely to be depleted in the next century (Yoon et al.2010). Finding alternative low cost clean energy sources represents an important challenge.

Building energy consumption currently accounts for over 40% of the total primary energy consumption in the U.S. and E.U. (Cao et al.2016). In France, it is classified as the most energy- consuming sector, which accounts for 43% of the total energy consumption and as the second most contributor to CO_2 gas emissions with a total contribution of 25%, just after the transportation sector (ADEME, 2013). Therefore, achieving a reduction in the total building energy consumption can provide key solutions to reduce energy demand and carbon emissions, which are considered as a serious threat to our societies.

Nevertheless, providing thermal comfort in buildings takes a major proportion of the total building energy consumption. Thus, enhancing the thermal insulation of building envelopes can significantly decrease building energy consumption. In this regard, insulation materials with a lower thermal conductivity will furtherly reduce heat flow crossing a building envelope which is responsible for 50-60% of total heat transfer in a building (Kumar et al.2020).

Therefore, optimization of thermal insulation for building envelope is crucial for thermal comfort, energy saving and reducing greenhouse gas emissions. While conventional building insulation materials are largely based on non-renewable resources requiring high

manufacturing energy, alternative sustainable insulation materials based on agro residues have been identified as low-embodied energy materials that simultaneously reduces energy demand and reinforces decarbonisation of the building sector.

Recently, many studies have been conducted on the mechanical, hygrothermal and acoustical performances of low-cost bio-based products for building insulation with promising results. In This regard, Badouard & coll. (2021) investigated the development and characterization of new bio-based materials based on viticulture by-products and potato starch for building insulation use. For this matter, four types of aggregates (grape pomace, stalks, skins, and crushed stalks) were used and mixed separately with potato starch. The starch/aggregate mass ratio was set at 20% for all mixtures and four types of composites were obtained and studied in terms of density, thermal conductivity, mechanical properties and sound absorption coefficient. Bourdot & coll. (2017) studied physical, mechanical and hygrothermal properties of a bio-composite made solely from wheat starch and hemp shives. The influence of hemp shive size and hemp/ wheat starch ratio on were investigated through an experimental approach. Mao & coll. (2017) studied hygrothermal properties of bio-insulation building materials based on bamboo fibers and bio-glues made up from bone glue mixed with sodium lignosulfonate. Bakatovich & coll. (2022) investigated the thermal insulation of materials based on reed and straw fibres bonded with sodium silicate and rosin. Bovo & coll. (2022) investigated thermal and acoustical performance of corncob for building insulation applications. Maalouf & coll. (2014) studied the hygrothermal behaviour of a hemp concrete building envelope under summer conditions in three French teams. Collet & coll. (2014) studied the impact of formulation, density and water content on the thermal performance of hemp concrete and observed a higher increase of the thermal conductivity with increasing density of hemp concrete in comparison with increasing water content, which had a lower effect. Colinart & coll. (2016) analysed the transient hygrothermal behaviour of a multi-layered hemp concrete wall coated with interior and exterior coarse plasters made of lime–sand mixtures. Other research works have focused on reinforcing mineral fibres with vegetal fibres in order to obtain a bio-composite, the main goal of this process being to benefit from the physical properties of the vegetal fibres and the mechanical properties of the mineral binder. Haba & coll. (2017) investigated the hygrothermal effect of a bio-composite insulation material for building application based on date palm concrete. Aouba & coll. (2015) studied the influence of incorporating wheat

straw to fired clay bricks on the thermal conductivity with reference to the bulk density, porosity and brick geometry. Hou & coll. (2017) showed that filling hollow concrete blocks with compressed straw reduces heat transfer and improve moisture-buffering performance.

In this regard, the sugar extraction process from sugar beets produces beet pulp that is considered as a low cost by- or waste product. Furthermore, the beet pulp production is continuously increasing with millions of tons of beet pulp pellets being produced yearly in France and Europe. Therefore, this low cost bio-based and locally available product happened to be an interesting substrate to be investigated for building insulation use.

Subsequently, various studies investigated a new bio-composite material based on sugar beet pulp and potato starch for building insulation use on material scale level. During his PhD studies, Karaky (2018) studied physical properties (morphology, porosity, density and particles size) of sugar beet pulp in addition to hygrothermal, mechanical and acoustical performances of different bricks made of different starch-beet pulp (S/BP) mass ratio (S/BP = 0.1, 0.2, 0.3 and 0.4.). The results showed that for an increase of the S/BP mass ratio, the thermal conductivity, mechanical properties, density and moisture buffering value increased and that the porosity and sound absorption coefficient of this bio-composite decreased. In this matter, a 0.4 mass ratio was found to be the optimal composition of S/BP in terms of the hygrothermal and mechanical properties and whereas a thermal conductivity at dry state was found equal to 0.075 (W/m. K) (Karaky et al. (2018); Karaky et al. (2019)). Moreover, Costantine and coll. (2020) compared the drying kinetics and mechanical properties of whole vs. hollowed bricks both having similar mixture composition of S/BP with a 40 % mass ratio compacted under a pressure equal to 0.044 MPa. The results showed that hollowed bricks had a more homogeneous and faster drying kinetics, higher elasticity modulus and compression resistance compared to whole bricks, showing that hollowed S/BP bricks can be used as a rigid material for building application.

The hollow block's structural configuration highly influenced the thermal characteristics and whereas Zhang & coll. (2017) studied the impact of rib width, number of rows with holes, number of holes, hole thickness and arrangement. The results showed that the thermal performance of the hollowed block with identical dimensions improved with the increase of number of rows with holes having a diameter not larger than 0.02 m.

For this reason and in order to study the optimal thermal performance of hollowed S/BP bricks with a constant mass ratio equal to 40%, numerical studies on thermal resistance using COMSOL v. 5.6 software were conducted on different hollowed bricks configurations. The results are then compared with analytical calculations based on the NF EN ISO norm 6946. (2017) and an optimal holes configuration in terms of thermal and mechanical performance was deduced. Afterwards, two experimental studies on the thermal performance were carried out on a 1m x 1m wall made of hollowed S/BP bricks cemented together by a 1cm layer of S/BP identical mix. The wall was inserted in a bi-climatic chamber THERMO^3 in order to measure its thermal resistance(3R, n.d.). Afterwards, highly precise thermal images were recorded by using the varioCAM HD (JENOPTIK, n.d.). For this matter, the S/BP wall was fixed from one side to the hot climatic chamber and exposed from the other side to ambient temperature, and heat transfer through the wall was analyzed by thermal imaging.

II. Numerical study

II.1 2D-numerical simulations of bricks

Hollow blocks are widely used in construction for having lighter weight and better insulation properties against heat and dampness. In order to achieve a better thermal performance of the S/BP bricks, a numerical study on holes distribution was conducted using the commercial software COMSOL v. 5.6.

The numerical simulations were set-up as a 2D simulation using the heat transfer in fluids and the surface-to-surface radiation physics interfaces and the built-in properties of air in the software COMSOL were used. Even though in a real façade the heat fluxes might be 3D in nature, a 2D simulation here was considered sufficiently accurate because the simulations were done on the level of one brick and the cross section of the brick is constant over its height.

The S/BP mixture was included as a solid (non-transparent for IR radiation), the air as a fluid (transparent for IR radiation; not including fluid flow; using the built-in properties of air) and the boundaries of the holes as diffuse surfaces with emissivity of 0.9 in order to exchange IR radiation through the holes. The governing equations for the heat transfer through the solids/fluids were defined by Eq. (1) and Eq. (2):

$$\nabla \cdot q = 0 \quad (1)$$

$$q = -\lambda \nabla T \quad (2)$$

155

156 With q (W/m^2) the heat flux density vector, λ (W/m.K) the thermal conductivity and *T* (K)
157 the temperature.

158 The surface-to-surface radiation heat transfer through the air-filled holes was governed by
159 Eq. (3) to Eq. (8):

$$J = \varepsilon e_b(T) + \rho_d G \quad (3)$$

$$\varepsilon + \rho_d = 1 \quad (4)$$

$$G = G_m(J) + G_{amb} \quad (5)$$

$$G_{amb} = F_{amb}\varepsilon_{amb} e_b(T_{amb}) \quad (6)$$

$$e_b(T) = n^2 \sigma T^4 \text{ with } n = 1 \quad (7)$$

$$q_{r,net} = \varepsilon\big(G - e_b(T)\big) \quad (8)$$

160 with *J* (W/m^2) the surface radiosity, ε (-) the surface emissivity, $e_b(T)$ (W/m^2) the blackbody
161 total emissive power, ρ_d (-) the surface reflectivity, *G* (W/m^2) the surface irradiation, $G_m(J)$
162 (W/m^2) the mutual surface irradiation, Gamb (W/m^2) the ambient irradiation, F_{amb} (-) the
163 ambient view factor, ε_{amb} (-) the ambient surface emissivity, *n* (-) the transparent media
164 refractive index, σ (W/(m^2.K^4)) the Stefan-Boltzmann constant, $q_{r,net}$ (W/m^2) the net
165 radiative heat flux density.

166 The boundary condition on the warm side of the brick was a heat flux boundary with a
167 temperature of 20˚C and surface heat transfer coefficient equal to 7.8 W/m^2.K while the
168 boundary on the cold side was a heat flux boundary with a temperature of 0˚C and surface
169 heat transfer coefficient equal to 25 W/m^2.K. The equations governing the heat flux
170 boundaries were defined by Eq. (9) and Eq. (10):

$$-n \cdot q = q_0 \quad (9)$$

$$q_0 = h(T_{ext} - T) \quad (10)$$

With $\boldsymbol{n}$ the normal vector, q_0 (W/m^2) the heat flux density on the surface, h (W/m^2.K) the surface heat transfer coefficient, T_{ext} (K) the temperature of the surrounding air and T (K) the temperature of the surface.

The mesh was a physics-controlled mesh with 'finer' mesh size as defined in the COMSOL software (see figure 1). This resulted in a total of 7498 triangular mesh elements.

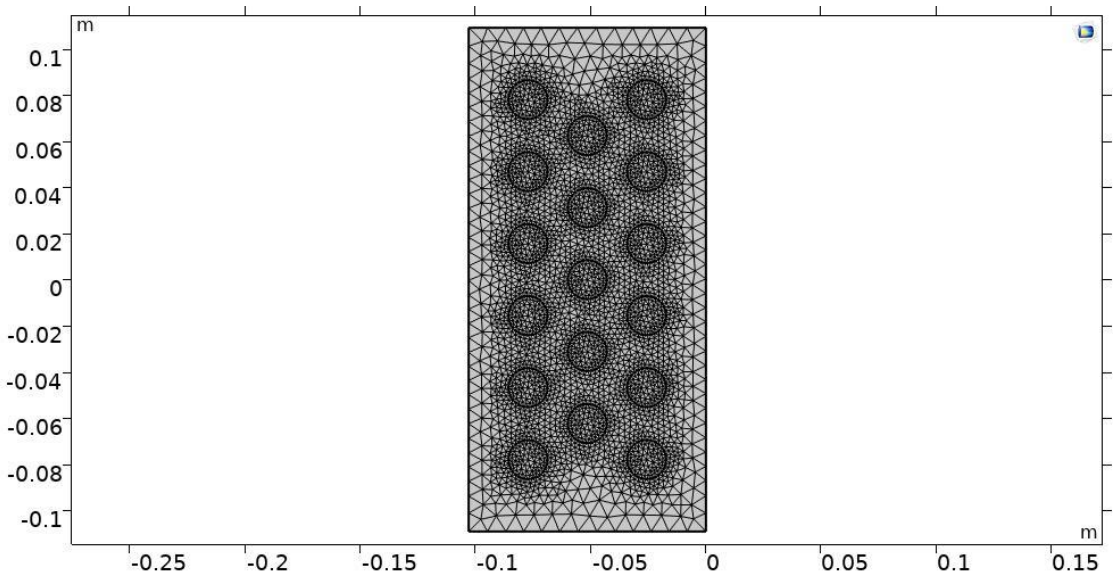

Figure. 1. Physics-controlled mesh for "finer" mesh size in COMSOL of the design for i=3 and j=6

The thermal conductivity of S/BP composite was measured experimentally using ISOMET 2114 Applied Precision (APPLIED PRECISION, n.d.). For this matter, an electrical resistor generating a defined heat flow was inserted in direct contact into the studied sample and temperature measurements were taken periodically.

Four cubical samples (10x10x10 cm3) of the S/BP composite were elaborated with the same manufacturing process of the bricks used in this study. Before measurements, samples were dried using a climatic chamber MKF 720 Binder (BINDER, n.d.) at 50 ◦C and 10% RH then cooled at 23 ◦C and 50 % RH for two weeks until stabilization. Afterwards, each sample was tested alone and covered during the test in order to avoid humidity variation. An average thermal conductivity equal to 0.09 W/m.K was obtained and used in our study.

The density and specific heat of the S/BP mixture were set equal to 360 kg/m^3 and 1450 J/kg.K respectively as previously measured (Karaky 2018).

With respect to the above mentioned conditions, 15 different simulations, each with a different holes configuration were run on a S/BP hollowed bricks with fixed dimensions (L = 21.85 cm, w = 10.3 cm and h = 5.6 cm) and equal holes diameters (D=1.7 cm) filled with air. The thermal resistance and equivalent thermal conductivity of the entire brick was deduced from each simulation.

While "i" refers to the number of rows with holes and "j" refers to the number of holes in a row and for "i" greater than 1, the configuration j/j-1 represents that the first row contains "j" holes while the second row contains "j-1" holes and the configuration is repeated for the following rows as shown in table 1.

For a configuration i=3 and J=6, a schematic representation of a hollowed brick is shown in Fig. 2.

Table 1
Total number of holes for different holes configuration.

i \ j/j-1	0/0	2/1	4/3	6/5	8/7
1	0	2	4	6	8
3	0	5	11	17	23
5	0	8	18	28	38

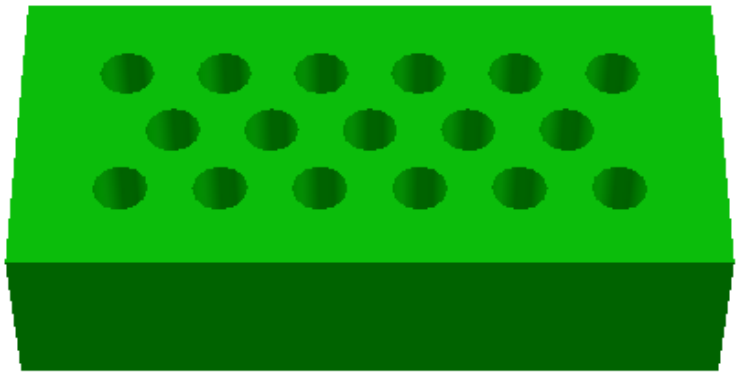

Figure. 2. Hollow brick design for i=3 and j=6

II.1.1 Thermal performance under steady state

Table 2 and 3 show the equivalent thermal conductivity and thermal resistance of S/BP brick for each hole configuration respectively. Fig. 3 and Fig. 4 show the impact of the total

number of holes on the equivalent thermal resistance and thermal conductivity respectively. The results show that the thermal resistance of the S/BP brick increases with increasing number of holes in a row and with the number of rows with holes. This can be explained by the fact that the brick in that case contains more air with a lower effective thermal conductivity than that of S/BP. The equivalent thermal conductivity of the brick equals 0.09 W/m.K if holes are absent; this corresponds to the thermal conductivity of S/BP. For our study and in order to meet all the requirements described above, a configuration with 17 holes was chosen for i=1 and j=6 and an equivalent thermal conductivity and thermal resistance were obtained respectively equal to 0.0873 W/m.K and 1.180 m^2.K/W.

Table 2

Equivalent thermal conductivity (W/m.K) of S/BP brick for different holes configuration.

j/j-1 / i	0/0	1/2	3/4	5/6	7/8
1	0.0900	0.0897	0.0894	0.0890	0.0887
3	0.0900	0.0892	0.0883	0.0873	0.0864
5	0.0900	0.0887	0.0872	0.0856	0.0841

Table 3

Equivalent thermal resistance (m^2.K/W) of S/BP brick for different holes configurations

j/j-1 / i	0/0	1/2	3/4	5/6	7/8
1	1.144	1.149	1.153	1.157	1.161
3	1.144	1.155	1.167	1.180	1.193
5	1.144	1.161	1.182	1.203	1.225

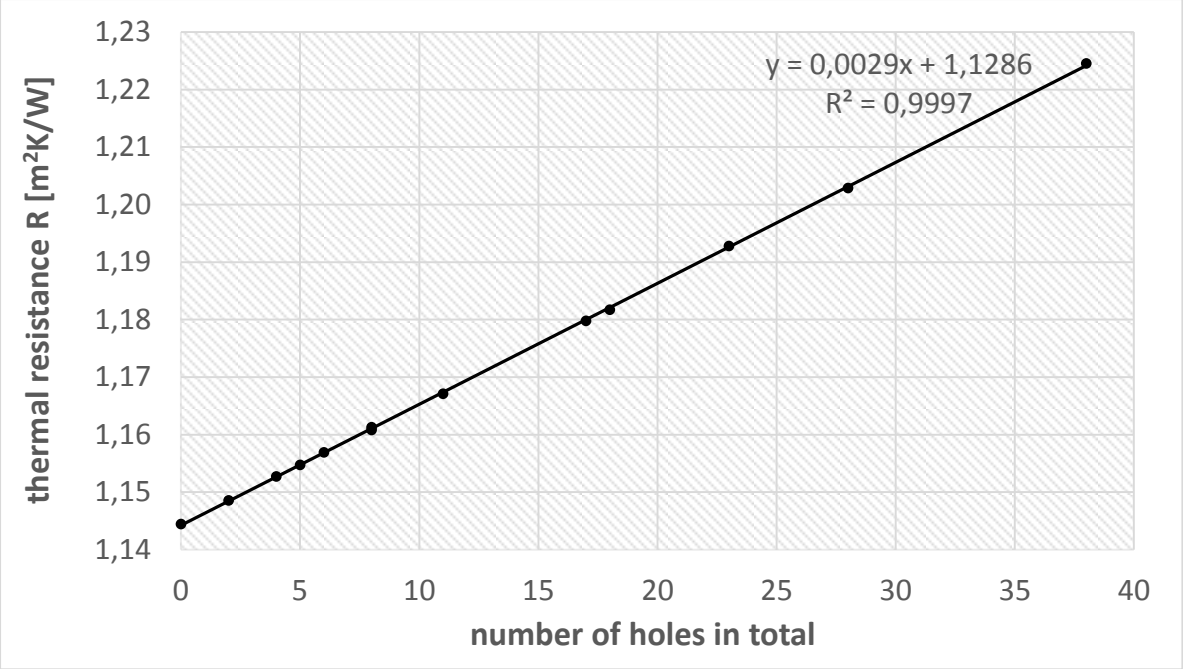

Figure. 3. Impact of holes number in a S/BP brick on the equivalent thermal resistance

226

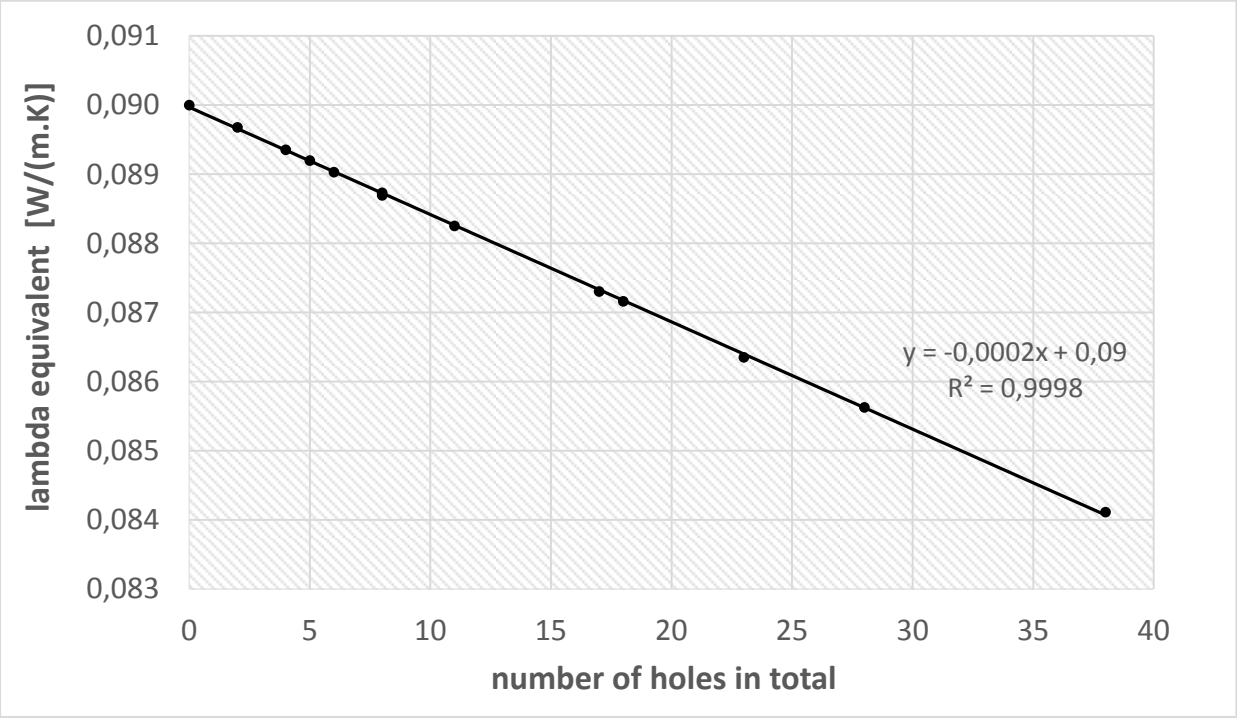

Figure. 4. Impact of holes number in a S/BP brick on the equivalent thermal conductivity

227 **II.2 Analytical calculations**

228 According to the NF EN ISO 6946 (2017), the thermal performance calculation of a
229 hollowed construction component consisting of thermally homogenous and heterogeneous
230 layers can be carried out while referring to the simplified calculation method. The thermal

resistance of each homogenous and heterogeneous part of the building wall is determined and then associated all together in order to obtain the equivalent thermal resistance of the wall and its equivalent thermal transmittance. To obtain the equivalent thermal resistance, a perforated S/BP brick was simplified as a 2D model as shown in Fig. 5. We proceeded by calculating the thermal resistance of a cylindrical hole in a first step, and then the thermal resistance of the S/BP composite based on the norm mentioned above from which the equivalent thermal resistance of a whole brick was concluded.

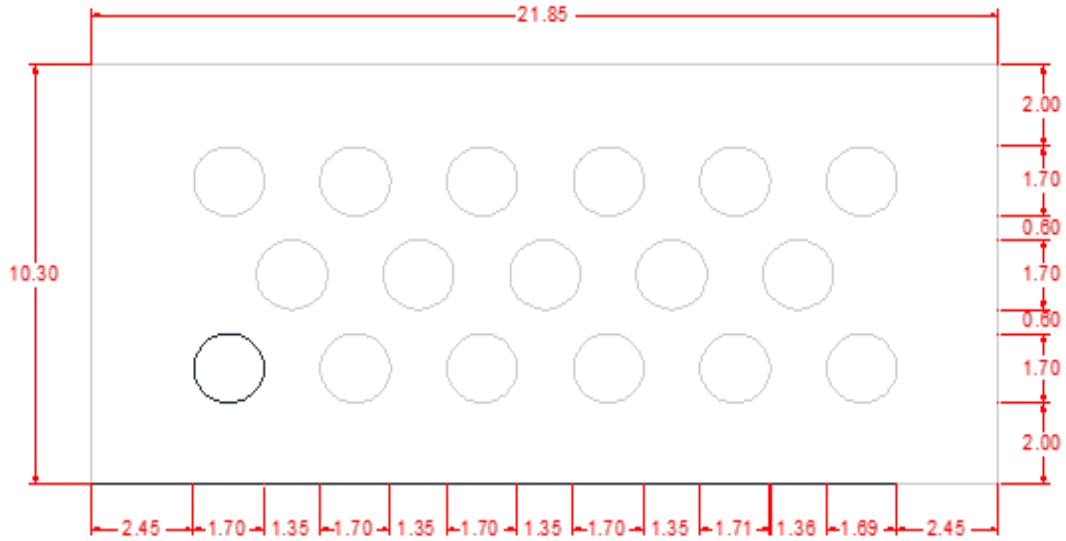

Figure. 5. S/BP brick dimensions

II.2.1 Thermal resistance of a cylindrical hole

According to the NF EN ISO 6946 (2017), air spaces with a thickness up to 0.3 m can be considered as thermally homogeneous. For a small air space having its width less than 10 times its thickness and for a thickness that does not exceed 0.05 m and for the air space not exchanging air with the interior environment, the thermal resistance for this air space can be obtained by Eq. (11) to Eq. (15):

$$Ra_{x,y} = \frac{1}{ha_{x,y} + hr_{x,y}} \quad (11)$$

$$\Delta T\ hole_{x,y} = Th\ hole_x - Tc\ hole_y \quad (12)$$

$$\Delta T\ average\ hole_{x,y} = \frac{Th\ hole_x + Tc\ hole_y}{2} \quad (13)$$

$$ha_1 = 1.25 \quad if \quad \Delta T_{hole} < 5K$$

$$ha_2 = 0.73\ \Delta T_{hole}/3 \quad if \quad \Delta T_{hole} > 5K$$

$$ha_3 = \frac{0.025}{dx,y}$$

$$ha_{x,y} = maximum\ value\ of\ (ha_1, ha_2, ha_3) \quad (14)$$

$$and\ hr_{x,y} = \frac{4\sigma\ (\Delta T average\ hole_{x,y})\text{^}3}{\frac{1}{\varepsilon_x}+\frac{1}{\varepsilon_y}-2+\frac{2}{1-\frac{dx_y}{bx_y}+\sqrt{1+\left(\frac{dx_y}{bx_y}^2\right)}}} \quad (15)$$

Moreover, it is assumed that the surfaces enclosing the air space are considered to have high hemispherical emissivity in all directions equal to 0.9; therefore $\varepsilon_x = \varepsilon_Y = 0.9$.

Table 4 shows the thermophysical properties of dry air at atmospheric pressure and T= 283.15 K. The thermal conductivity of the S/BP mixture was set equal to 0.09 W/m.K and as for density and specific heat of the composite, values were set at 360 kg/m^3 and 1450 J/kg.K respectively as found in the PHD thesis of Karaky. (2018) for a ratio of S/BP equal to 0.4.

Table 4

Thermophysical properties of dry air at atmospheric pressure and T= 283.15 K

ρ (kg/m^3)	Cp (j/kg.k)	λ (w/m.k)	μ (kg/m^2.s)	V (m^2/s)	β (K^{-1})	Pr	α (m^2/s)	Reference
1.246	1006	0.02439	1.778E-05	1.426E-05	0.0035	0.7336	1.944E-05	Cengel & Ghajar (2020)

In order to simplify the geometry of the uniform cylindrical cavities for the heat transfer calculation, having each a diameter of 1.7 cm and a height of 5.6 cm, an equivalent thickness of the cylindrical cavities was used as shown in Fig. 6, and a simplified geometrical scheme for the air cavity and the S/BP brick were adopted, as shown in Fig. 7 and Fig. 8. respectively (Kočí et al. 2015).

262 Where T1 and T2 are the average surface temperatures of (T1; T1”) and (T2’, T2”)
263 respectively, D is the hole diameter and L is the equivalent length which represents the
264 dimension of the air cavity in the direction of the heat flux which is obtained by Eq. (16):

$$L = 0.785\,D \quad (16)$$

265

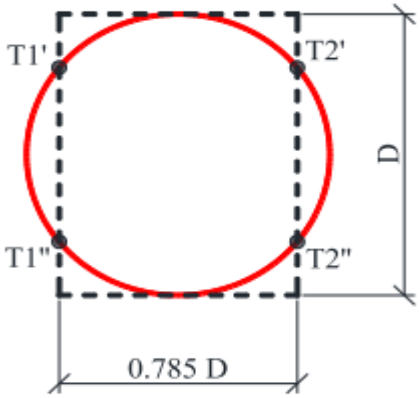

Figure. 6. Determination of the equivalent thickness of a cylindrical cavity

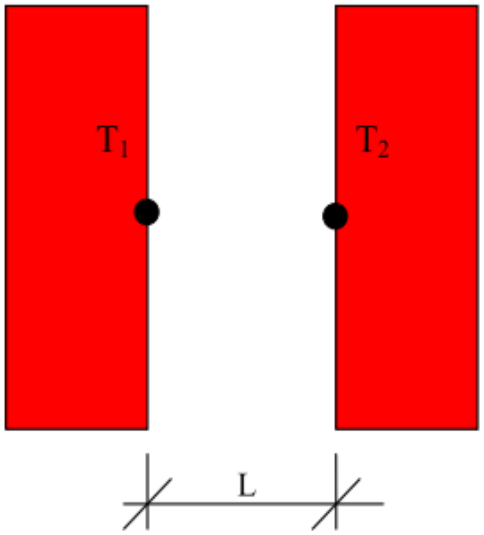

Figure. 7. Simplified scheme of the air cavity

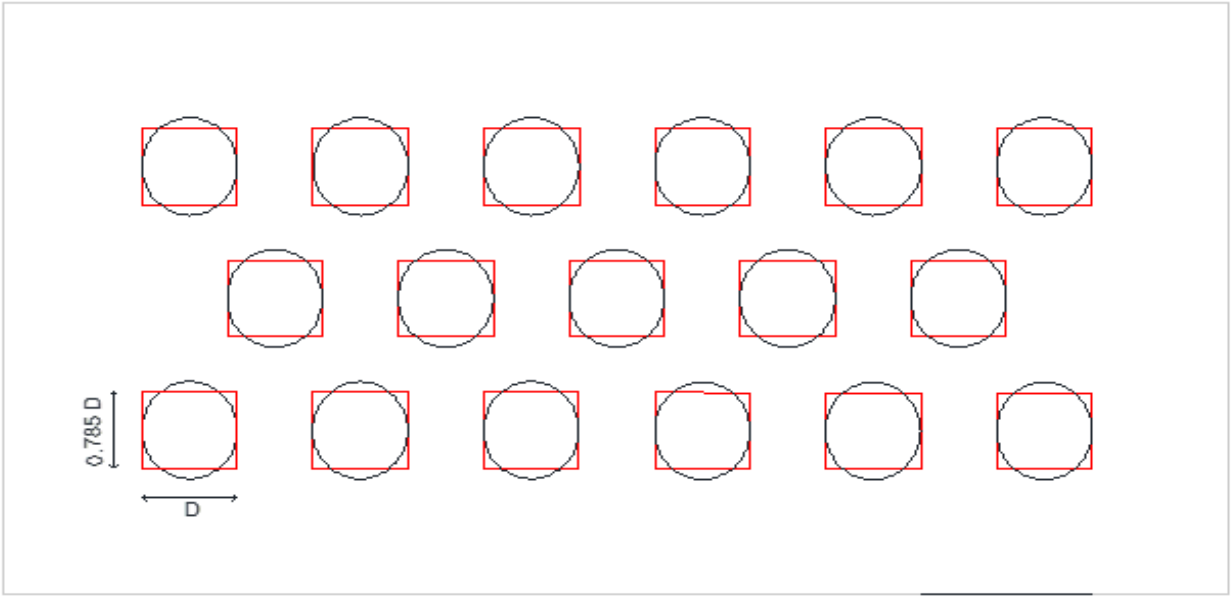

Figure. 8. Equivalent simplified scheme of S/BP brick

II.2.2 Thermal resistance of the S/BP composite

The microstructure analysis of the S/BP bio-composite mixture was done by Costantine and coll. (2020) using scanning electron microscope (SEM) imaging. The results showed that S/BP bio-composite had a rugged and open structure and the starch granules were no longer visible and a good compatibility was seen between the two polymeric constituents. Moreover, Karaky & coll. (2018) studied the porosity of the S/BP bio-composite based on the cyclohexane insertion method while using a pycnometer and a porosity equal to 70.6% was found for a S/BP ratio of 0.4. It is shown that the body itself is porous, but the dimensions of the pore are so small that radiation and convection inside these pores can be neglected thus it is considered that heat transfer occurs only through conduction (Kočí and coll. (2015).

The thermal resistance of this bio-composite can be obtained by Eq. (17):

$$Rx,y = \frac{ex,y}{\lambda m} \qquad (17)$$

Where Rx,y is the thermal resistance of the S/BP brick between points x and y (m^2.K/W), ex,y is the thickness of the S/BP brick limited by points x and y (m) and λm is the thermal conductivity of the S/BP bio-composite (W/m.K).

II.2.3 Heat flux calculation

Assuming a unidimensional (1D) heat transfer, the total heat flux through the brick is equal to the sum of the heat fluxes through each section of the brick, which is divided into 23 sections depending on its geometry and holes distribution as shown in Fig. 9.

The heat flux through each section is assumed to be constant from the bottom to the top of the brick sections. Therefore, the total heat flux ΦT through the S/BP brick can be calculated as follows by using Eq. (18) to Eq. (24):

$$\Phi T = \sum_{i=1}^{23} \Phi i, Si \qquad (18)$$

$$\Phi i = \frac{Ti - Te}{Ri} \quad (19)$$

$$Ri = Rs,i + \sum Rx,y + \sum Ra,x,y + Rs,e \quad (20)$$

$$Rs,i = \frac{1}{hi} \quad (21)$$

$$Rs,e = \frac{1}{he} \quad (22)$$

$$\Phi i,Si = \Phi i \; x \; Si \quad (23)$$

$$\Phi T = 2 \; x \; \Phi 1,S1 + 2 \; x \; \Phi 2,S2 + 10 \; x \; \Phi 3,S3 + 5 \; x \; \Phi 4,S4 + 4 \; x \; \Phi 2',S2' \quad (24)$$

Whereas, ΦT is the total unidirectional heat flux (W) crossing the total surface ST (m^2) of the S/BP brick and $\Phi i,Si$ is the heat flux density Φi crossing through the section Si of the brick having Ri as an equivalent thermal resistance (m^2.K/W), as shown in Fig. 9.

Ti, Te, Rs,i, Rs,e, hi and *he* are respectively the internal temperature (K), the external temperature (K), the inner surface thermal resistance due to convection (m^2.K/W), the outer surface thermal resistance due to convection (m^2.K/W), the convective heat transfer coefficient of the internal hot wall side (W/m².K) and the convective heat transfer coefficient of the external cold wall side (W/m².K) respectively.

Considering that *Ti* = 20 °C and *Te* =0°C and solving the above equations by an iterative calculation procedure as described by Laaroussi and coll. (2017), a total heat flux ΦT is obtained equal to 0.176 W through the total brick surface equal to 0.0122 m^2.

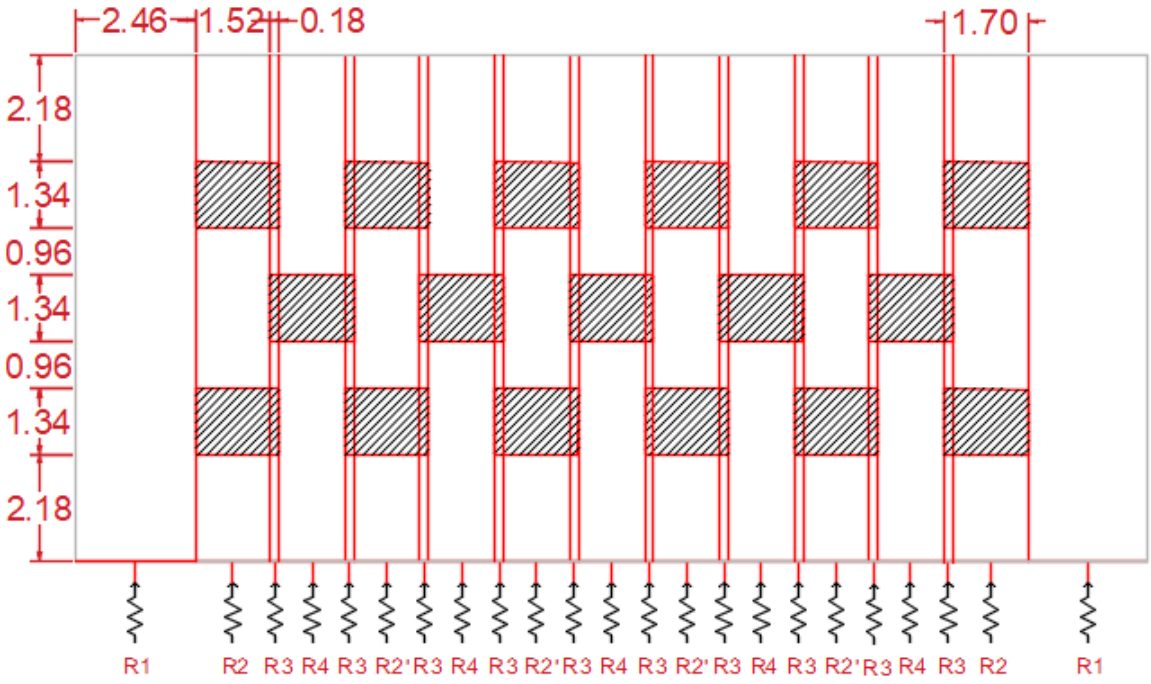

Figure. 9. Equivalent simplified scheme of S/BP brick

II.2.4 Equivalent thermal resistance of S/BP brick

The equivalent thermal resistance of S/BP can be concluded as follows, by using Eq. (25) and Eq. (26):

$$R\ brick = \frac{1}{U} - Rs,i - Rs,e \quad (25)$$

$$U = \frac{\Phi\ T}{ST(Ti - Te)} \quad (26)$$

Where U is the thermal transmittance W/(m²·K) and ST is the total surface of the S/BP brick (m²) crossed by the heat flux ΦT. Therefore, the calculation described above leads to U = 0.721 W/m². K and R brick =1.218 m².K/W.

III. Experimental set up

III.1 Bricks manufacturing

In this work, bricks were constructed in a similar matter as described by Costantine et al. (Costantine et al.2020) and an optimal S/BP 40% mass ratio of was adopted as shown by Karaky et al. (2018, 2019). A water/beet pulp mass ratio was chosen equal to 2.5 and dry beet pulps were soaked in water for 2 hours until saturation. In a next step, potato starch granules were mixed manually for 10 min with the saturated wet pulps until complete

homogenization. Afterwards, the obtained mixture was placed in an autoclave and heated for 30 min at 120˚ C and then poured into wooden molds. All bricks were produced and compacted under a pressure of 0.044 MPa, then frozen at -80˚C and dried using a freeze-dryer which provided a more effective drying with a minimal shrinkage percentage of 2.5 % while preserving a higher sample surface quality as compared with pulsed hot air drying.

III.2 Wall construction

In order to study the thermal performance at the wall scale, a 100 cm x 100 cm wall having a surface area equal to 1 m^2 and a thickness equal to 10.3 cm was constructed using S/BP hollowed bricks. All bricks used to construct the wall are considered uniform having the same dimensions (L = 21.85 cm, w = 10.3 cm and h = 5.6 cm with internal holes diameters D = 1.7 cm. The bricks were cemented together by a 1cm layer of S/BP identical mix for the sake of material homogeneity. The binder used had similar material composition to the S/BP bricks with the same mass ratio equal to 0.4. The resulting wall was dried at ambient temperature for several months in a ventilated room with regular fan ventilation prior to study. The wall was perfectly fitted and sealed into a wooden frame as shown in Fig. 10 and Fig. 11, whereas only an opening of 70 cm x 70 cm was maintained in the wooden enclosure on the center of both sides of the wall, which represents the area in contact with the hot and cold sides of the bi-climatic chamber. Therefore, the heat exchanged between the two hot and cold chambers through the wall was limited to this area only since all lateral surfaces of the wall are well insulated in order to prevent any lateral heat exchange with the environment.

Figure. 10. side enclosure with wooden frame

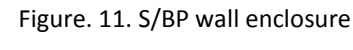

Figure. 11. S/BP wall enclosure

335

336 **III.3 Thermal performance**

337 **III.3.1 Equivalent thermal resistance of a S/BP brick**

338 After production, the S/BP wall was inserted and tightened between the two
339 enclosures of a bi-climatic chamber THERMO[3] as shown in Fig. 12. This device allowed
340 to measure the heat passing through the wall under different thermal conditions as
341 shown in Fig. 13. Each chamber was insulated with a 10 cm thickness of polyurethane,
342 and was equipped with 8 digital temperature sensors distributed throughout the
343 volume and on the surface of the wall to be tested. Temperature uniformity was
344 ensured by mechanical ventilation without disturbing the natural convection which was
345 maintained between the surface wall and surrounding zones.

346 The density of the heat flux through the wall inserted inside the bi-climatic chamber can
347 be obtained by using the following Eq. (27):

$$\Phi p = \frac{Pe}{Sm} \qquad (27)$$

348 Where *φp, Pe* and *Sm* are the density of the heat flux (W/m²), the electrical power
349 developed by the heating chamber of the device (W) and the surface of the S/BP wall in
350 contact with the heating chamber (m^2) respectively.

351 Finally, the thermal resistance of the S/BP wall was calculated using Eq. (28) while the
352 equivalent thermal resistance of this wall was calculated using Eq. (29) as follows:

$$R = \frac{Sm\,.(Tc - Tf)}{Pe} \qquad (28)$$

$$Req = R + \frac{1}{hc} + \frac{1}{hf} \qquad (29)$$

353 Where *R, Tc, Tf* are the thermal resistance of the S/BP wall (m². K/W), the temperature of
354 the wall surface in contact with the hot zone, the temperature of wall surface in contact
355 with the cold zone respectively and *Req, hc, hf* are the equivalent thermal resistance of the
356 S/BP wall (m².K/W), the convective heat transfer coefficient on the hot wall side (W/m².K)
357 and the convective heat transfer coefficient on the cold wall side (W/m².K) respectively.

Table 5 shows the thermal conditions imposed in the bi-climatic chamber at steady state while the experimental results for the thermal properties of the S/BP wall and the equivalent thermal properties of the same wall are shown in tables 6 and 7 respectively.

Table 5

Thermal conditions imposed in the bi-climatic chamber at steady state

Sm (m^2)	Hot air average temperature (°C)	Tc (°C)	Cold air average temperature (°C)	Tf (°C)	Heat flux (W)
0.64	27.96	26.15	-0.01	1.84	14.19

Table 6

Conditions imposed in the bi-climatic chamber at steady state regime

R (m².K/W)	Wall thermal transmittance (W/m².K)	Equivalent wall thermal conductivity (W/m.K)	Heat flux density (W/m²)
1.10	0.91	0.094	22.18

Table 7

Equivalent S/BP wall thermal properties

Req (m².K/W)	Equivalent wall Thermal transmittance (W/m².K)	hc (W/m².K)	Hf (W/m².K)
1.26	0.79	12.2	12.0

Figure. 12. S/BP wall insertion in the Thermo[3] device

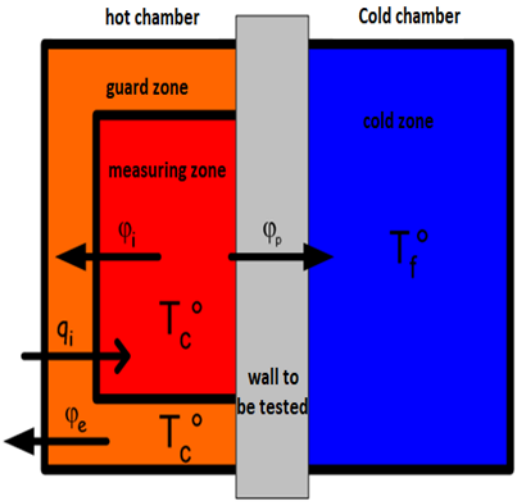

Figure. 13. heat transfer inside a bi-climatic chamber

Experimental results show a thermal resistance of the S/BP composite equal to 1.10 m².K/W which is slightly lower compared to the results obtained by the analytical calculations (1.218 m^2.K/W) and numerical study (1.180 m².K/W), which can be probably attributed to minor measurements inaccuracies. The equivalent thermal resistance comparison between numerical and experimental of S/BP composite is shown in Fig. 14.

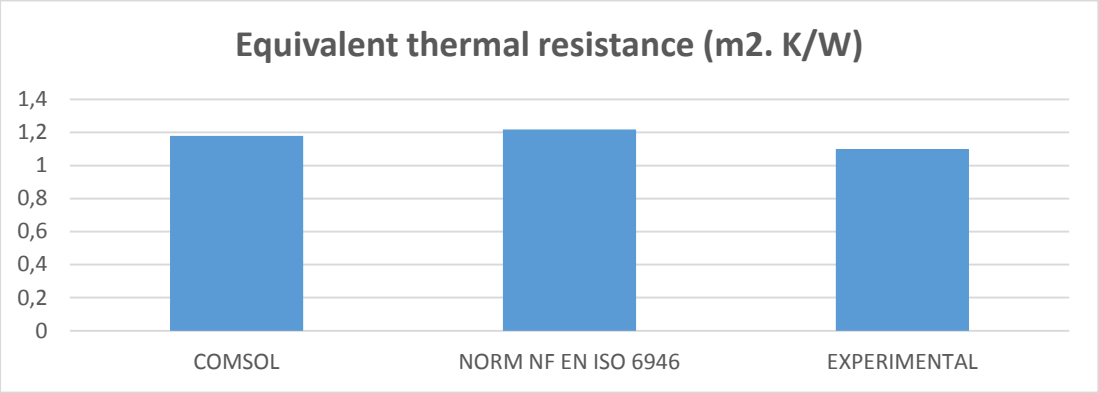

Figure. 14. Equivalent thermal resistance comparison between numerical and experimental of S/BP composite

III.3.2 Thermal imaging

The S/BP wall originally stored at 17°C and RH 50% for more than a month, was fixed to the hot climatic chamber of the Thermo[3] device on one side and kept exposed to a constant ambient temperature equal to 17°Con the other side. A constant temperature of 40°C and RH 50% inside the hot chamber was imposed to the air in contact with the surface of the wall and additionally, all lateral surfaces of the wall were well insulated in order to prevent any lateral heat exchange with the environment as shown in Fig. 15.

Figure. 15. S/BP wall fixed from one side to the hot climatic chamber
and exposed to ambient temperature from the other side

In order to analyze the heat transfer and temperature variation and distribution over the entire exposed wall surface, highly precise thermal images were recorded using the varioCAM HD thermography camera, which combines high-resolution image sensors equipped with optomechanical resolution enhancement technology. This type of equipment is widely used in building thermography for tracing heat and energy losses in the thermal insulation of buildings with a non-contact process. The thermography camera has a maximum image resolution of 2048x1536 IR pixels (RE mode), a spectral range between 7.5 µm and 14 µm, a temperature measuring range between -40°C and + 1200°C, a thermal resolution < 50 mK and an accuracy of 1.5 K or 1.5% (JENOPTIK, n.d.). It was placed in front of the surface of the S/BP wall exposed to the ambiance and hourly thermal images were taken as shown in Fig. 16

Figure. 16. Thermal imaging recording of S/BP wall surface exposed to ambient temperature

While table 8 shows the recorded values of the minimum, maximum and average wall surface temperature of the side exposed to ambient temperature. Fig. 17 shows an increase of only 3.21°C of the average surface wall temperature after 450 minutes for a 23°C air temperature difference between both wall sides, which reflects the remarkable thermal performance of the studied wall.

Table 8

Maximum, minimum and average wall surface temperature of the side exposed to the ambient temperature obtained by thermal imaging with respect to time in minutes

	0	90	120	180	240	300	360	450
Tavg (˚C)	17.68	18.45	18.79	19.50	19.74	20.21	20.58	20.89
Tmin (˚C)	17.07	16.97	17.64	18.57	18.74	19.06	19.28	19.59
Tmax(˚C)	18.07	19.41	19.91	21.29	22.04	22.78	23.36	23.50

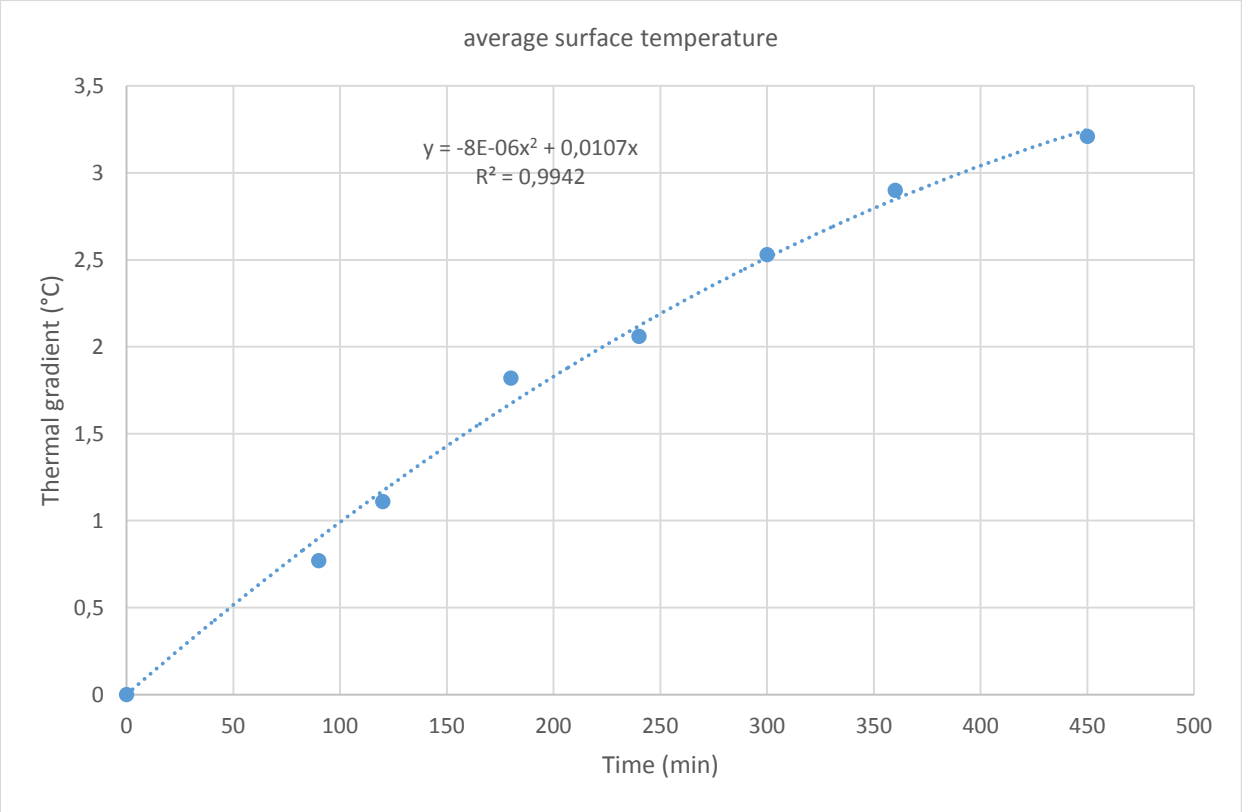

Figure. 17. Average surface temperature variation of side wall exposed to ambient temperature

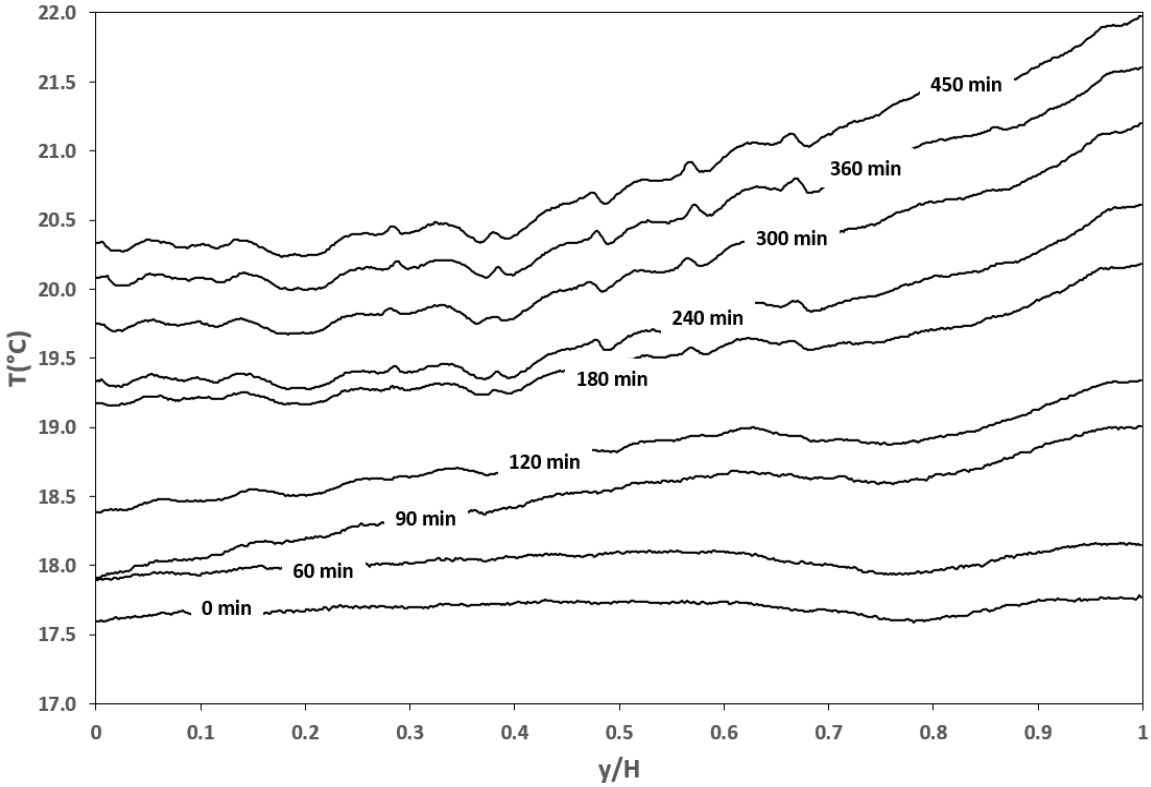

Figure. 18. Wall surface temperature gradients with respect to height and time

Moreover, with H symbolizing total height of the surface wall exposed to ambient temperature and y/H symbolizing partial wall heights varying from 0 to 1 (bottom and top of the wall respectively), Fig. 18 reveals various surface temperature gradients in terms of wall elevation with respect to time. The results show an increase of surface temperature with height which can be explained by the natural convection phenomenon and whereas a higher temperature difference between the bottom and top of the wall was recorded with time due to average wall temperature increase. Finally, Fig. 19 shows the recorded images by thermography reflecting the temperature variation all over the wall surface exposed to the ambient temperature with time.

The results show a nearly uniform temperature distribution horizontally with a slight variation at the center of the perforated S/BP brick mainly due to the presence of air inside and another slight variation at the joints of the brick probably due to small difference in material amounts.

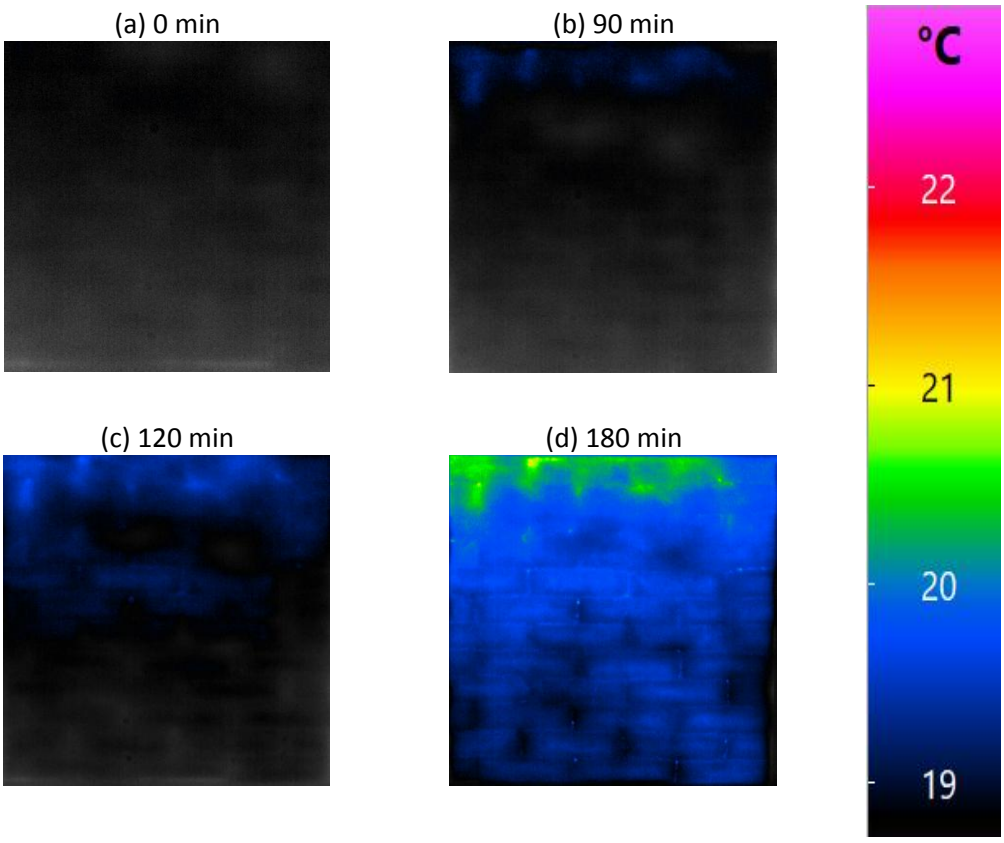
(a) 0 min
(b) 90 min
(c) 120 min
(d) 180 min
°C
22
21
20
19

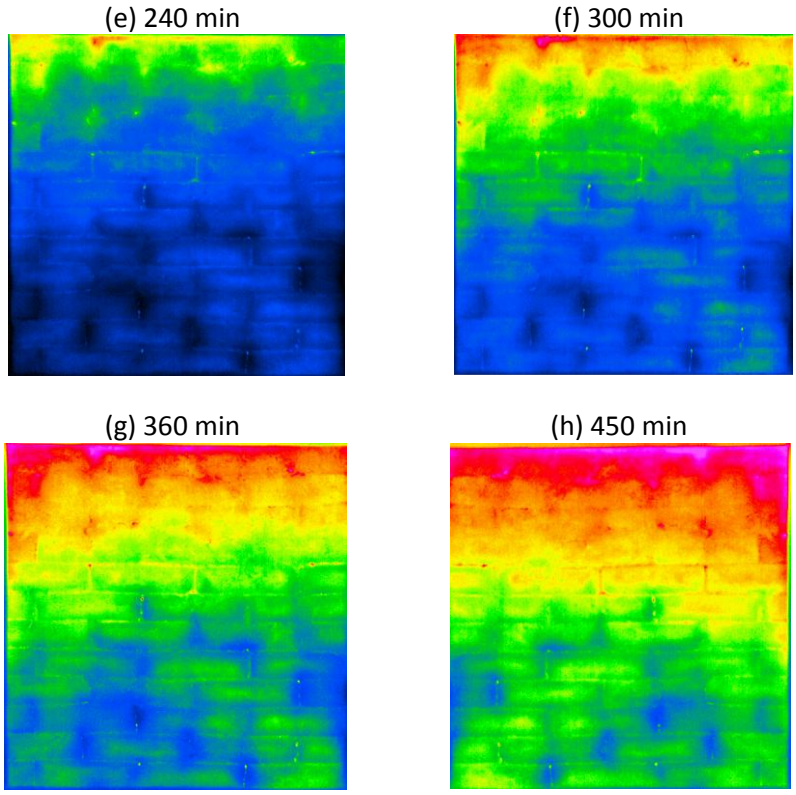

441 Figure. 19. Visible images by thermography that depict the distribution of temperature differences on the S/BP
442 wall surface exposed to ambient temperature and recorded at: (a) 0 min, (b) 90 min, (c) 120 min, (d) 180 min,
443 (e) 240 min, (f) 300 min, (g) 360 min, (h) 450 min.

444

445 **IV. Results and discussions**

446 In this study, the thermal conductivity of the S/BP bio-composite was numerically,
447 analytically and experimentally investigated. An equivalent thermal conductivity is obtained
448 almost identical for all results around (ca 0.09 W/(m.K)).

449 Beet-pulp/starch composite presented a thermal conductivity slightly lower than other bio-
450 based composites thermal conductivities ranging from 0.0693 to 0,0793 W/ (m.K) for grape
451 by-products/starch (Badouard et al. 2021), 0.06 to 0.07 W/ (m.K) for hemp/Wheat starch (
452 Bourdot et al. 2017), 0.055 to 0.088 W/ (m.K) for bamboo fiberboards/Bone glue mixed with
453 sodium lignosulfonate (Mao et al. 2017), 0.047 to 0.055 W/ (m.K) for mixture of reed and
454 straw/Rosin obtained from pine resin (Bakatovich et al. 2022). All these studies revealed
455 that the thermal conductivities of bio-based composites highly depend on their type,
456 formulations and densities along with binder type and bio-composites to binder mass ratio.

Table 9 shows density and thermal conductivity comparison between the S/BP bio-composite, other natural bio-composites investigated for building insulation use and other conventional building insulation materials currently used in construction found in the literature.

Overall, it can be concluded that the S/BP bio-composite can be considered as an effective material for building insulation use.

Table 9
Density and thermal conductivity comparison of S/BP with other natural and conventional insulation materials used in construction.

Material	Density (kg/m^3)	Thermal conductivity (W/m.K)	References
Glass wool	10–100	0.03–0.05	Kumar & coll. (2020)
Rock wool	40–200	0.033–0.04	
Expanded Polystyrene	18–50	0.029–0.041	
Extruded Polystyrene	32–40	0.032–0.037	
Foamed Glass	100–200	0.038–0.055	
Cellulose	30–80	0.037–0.042	
Hemp concrete	300-500	0.0971-0.1659	Collet & coll. (2014)
Cellular concrete	600	0.14	Maalouf & coll. (2014)

Earth block	1850	1	
Solid brick	1950	0.87	
Concrete	2300	1.75	
Grape by-products/Starch	227-433	0.0693-0,0793	Badouard & coll. (2021)
Hemp/Wheat starch	182-187.9	0.06–0.07	Bourdot & coll. (2017)
Bamboo fiberboards/Bone glue mixed with sodium lignosulfonate	311-538	0.055-0.088	Mao & coll. (2017)
Mixture of reed and straw/Rosin obtained from pine resin	160-224	0.047-0.055	Bakatovich & coll. (2022)
Beet pulps/ Potato starch	360	0.094	This Study

V. Conclusions

This work focuses on the study of the thermal performance of a low cost and bio-sourced material based on starch and beet-pulp (S/BP) as building insulation material on a wall scale level. For this purpose, a numerical study was elaborated using the commercial software COMSOL in order to determine the best holes distribution profile for a high thermal resistance of a brick while at the same time satisfying a good mechanical behaviour. An equivalent thermal resistance equal to 1.180 m^2. K/W was obtained for a brick (21.85 cm x 10.3 cm x 5.6 cm) having a total number of 17 holes distributed in 3 rows. Afterwards, the obtained result was compared to an analytical calculation based on the norm NF EN ISO 6946 (2017) for the same brick configuration resulting in an equivalent thermal resistance equal to 1.218 m^2.K/W

In a later stage, an experimental thermal study was made on a S/BP brick wall with the same configuration elaborated above by inserting this wall in a bi-climatic chamber. A slightly lower equivalent thermal resistance of the wall equal to 1.10 m^2.K/W was obtained, which could be due to small measurements inaccuracies.

Therefore, the obtained results reflected a good agreement between the numerical and experimental results. Moreover, the results revealed that the studied S/BP composite had a high thermal performance compared to other insulation materials used in building construction.

Finally, highly accurate thermal imaging was performed on the S/BP brick wall exposed to a constant temperature of 40°C on one side and to ambient temperature of 17°C

on the other side in order to analyze the heat transfer by studying the distribution of the temperature differences on the S/BP wall surface. Promising results were obtained where a nearly uniform temperature distribution was found horizontally and an increase in temperature from the bottom of the wall to the top was shown due to natural convection. Moreover, the thermal images reflected the good thermal inertia of the wall since an increase of only 3.21°C of the average surface wall temperature was shown after 450 minutes of exposure to a constant temperature of 40°C while maintaining a steady room temperature of 17°C at constant relative humidity equal to 50%.

Further investigations are also ongoing using S/BP hollowed bricks at wall scale to study the hygric behaviour of this material.

VI. Acknowledgment

The authors would like to thank Crystal Union Company for providing the beet-pulp pellets necessary for the specimens manufacturing.

VII. References

Yoon, J., Sun, Y., & Rogers, J. A. (2010). Flexible Solar Cells Made of Nanowires/Microwires. In Semiconductor Nanomaterials for Flexible Technologies: From Photovoltaics and Electronics to Sensors and Energy Storage (First Edition). https://doi.org/10.1016/B978-1-4377-7823-6.00006-4

Cao, X., Dai, X., & Liu, J. (2016). Building energy-consumption status worldwide and the state-of-the-art technologies for zero-energy buildings during the past decade. *Energy & Buildings*, *128*, 198–213. https://doi.org/10.1016/j.enbuild.2016.06.089

ADEME. (2013). "Les Chiffres Clés Du Bâtiment Énergie - Environnement." Retrieved from http://www.ademe.fr/sites/default/files/assets/documents/chiffres-cles-batiment-edition-2013-8123.pdf.

Badouard, C., Bogard, F., Bliard, C., Lachi, M., Abbes, B., & Polidori, G. (2021). Development and characterization of viticulture by-products for building applications. *Construction and Building Materials*, *302*(July). https://doi.org/10.1016/j.conbuildmat.2021.124142

Bovo, M., Giani, N., Barbaresi, A., Mazzocchetti, L., Barbaresi, L., Giorgini, L., … Tassinari, P. (2022). Contribution to thermal and acoustic characterization of corn cob for bio-based building insulation applications. *Energy and Buildings*, *262*, 111994. https://doi.org/10.1016/j.enbuild.2022.111994

534 Maalouf, C., Le, A. D. T., Umurigirwa, S. B., Lachi, M., & Douzane, O. (2014). Study of
535 hygrothermal behaviour of a hemp concrete building envelope under summer conditions in
536 France. *Energy and Buildings*, *77*, 48–57. https://doi.org/10.1016/j.enbuild.2014.03.040

537 Collet, F., & Pretot, S. (2014). Thermal conductivity of hemp concretes: Variation with
538 formulation, density and water content. *Construction and Building Materials, 65, 612–619.*
539 http://dx.doi.org/10.1016/j.conbuildmat.2014.05.039

540 Colinart, T., Lelievre, D., & Glouannec, P. (2016). Experimental and numerical analysis of
541 the transient hygrothermal behavior of multilayered hemp concrete wall. *Energy and*
542 *Buildings, 112, 1–11.* http://dx.doi.org/10.1016/j.enbuild.2015.11.027

543 Haba, B., Agoudjil, B., Boudenne, A., & Benzarti, K. (2017). Hygric properties and thermal
544 conductivity of a new insulation material for building based on date palm concrete.
545 *Construction and Building Materials*, 154, 963–971.
546 http://dx.doi.org/10.1016/j.conbuildmat.2017.08.025

547 Aouba, L., Coutand, M., & Perrin, B. (2015). Predicting thermal performance of fired clay
548 bricks lightened by adding organic matter*: Improvement of brick geometry*. Building Physics.
549 38(6) 531–547. https://doi.org/10.1177/1744259115571078

550 Hou, S., Liu, F., Wang, S., & Bian, H. (2017). Coupled heat and moisture transfer in hollow
551 concrete block wall filled with compressed straw bricks. *Energy & Buildings*, *135*, 74–84.
552 https://doi.org/10.1016/j.enbuild.2016.11.026

553 Karaky, Hamzé. (2018). "Élaboration et Caractérisation Physique et Hygrothermique d'un
554 Agro-Matériau à Base de Pulpe de Betterave et d'amidon." Thèse de l'Université de Reims-
555 Champagne-Ardenne.

556 Karaky, H., Id, C. M., Bliard, C., Moussa, T., Wakil, N. El, Lachi, M., & Polidori, G. (2018).
557 Hygrothermal and Acoustical Performance of Starch-Beet Pulp Composites for Building
558 Thermal Insulation.*Materials, 2018, 11, 1622.* https://doi.org/10.3390/ma11091622

559 Karaky, H., Maalouf, C., Bliard, C., Gacoin, A., Lachi, M., El, N., & Polidori, G. (2019).
560 Characterization of beet-pulp fiber reinforced potato starch biopolymer composites for
561 building applications. *Construction and Building Materials,203*, 711–721.
562 https://doi.org/10.1016/j.conbuildmat.2019.01.127

563 Costantine, G., Harb, E., Bliard, C., Maalouf, C., Kinab, E., Abbès, B., … Polidori, G.
564 (2020). Experimental characterization of starch / beet-pulp bricks for building applications:
565 Drying kinetics and mechanical behavior. *Construction and Building Materials*, *264*, 120270.
566 https://doi.org/10.1016/j.conbuildmat.2020.120270

567 Zhang, Y., & Wang, Q. (2017). Influence of Hollow Block's Structural Configuration on the
568 Thermal Characteristics of Hollow Block Wall. *Procedia Engineering*, *205*, 2341–2348.
569 https://doi.org/10.1016/j.proeng.2017.10.306

570 Kočí, J., Maděra, J., & Černý, R. (2015). A fast computational approach for the determination
571 of thermal properties of hollow bricks in energy-related calculations. *Energy*, *83*, 749–755.
572 https://doi.org/10.1016/j.energy.2015.02.084

573 NF EN ISO 6946. (2017). Composants et parois de bâtiments - Résistance thermique et
574 coefficient de transmission thermique - Méthodes de calcul. AFNOR 2017.

575 Laaroussi, N., Lauriat, G., Raefat, S., Garoum, M., & Ahachad, M. (2017). An example of
576 comparison between ISO Norm calculations and full CFD simulations of thermal
577 performances of hollow bricks. *Journal of Building Engineering*, *11*(March), 69–81.
578 https://doi.org/10.1016/j.jobe.2017.03.011

579 JENOPTIK. (n.d.), Handheld thermography cameras for highly precise thermal imaging.
580 Retrieved May 3, 2022, from https://www.jenoptik.com/products/cameras-and-imaging-
581 modules/ thermographic-camera/handheld-thermographic-camera .

582 3R. (n.d.), Cellule Thermique THERMO 3. Retrieved September 8, 2022, from https://3r-
583 labo.com/produit/thermo-3/

584 APPLIED PRECISION. (n.d.), Portable heat analyzer. Retrieved October 20, 2022, from
585 https://www.appliedp.com/product/isomet/

586 BINDER, (n.d.), Chambres d'essais climatiques. Retrieved September 8, 2022, from
587 https://www.binder-world.com/fr/produits/chambres-d%E2%80%99essais-climatiques/serie-
588 mkf/mkf-720

589 Mariano-Hernández, D., Hernández-Callejo, L., Zorita-Lamadrid, A., Duque-Pérez, O., &
590 Santos García, F. (2021). A review of strategies for building energy management system:
591 Model predictive control, demand side management, optimization, and fault detect &
592 diagnosis. *Journal of Building Engineering*, *33*(March 2020).
593 https://doi.org/10.1016/j.jobe.2020.101692

594 Rabbat, C., Awad, S., Villot, A., Rollet, D., & Andrès, Y. (2022). Sustainability of biomass-
595 based insulation materials in buildings: Current status in France, end-of-life projections and
596 energy recovery potentials. *Renewable and Sustainable Energy Reviews*, *156*.
597 https://doi.org/10.1016/j.rser.2021.111962

598 Kumar, D., Alam, M., Zou, P. X. W., Sanjayan, J. G., & Memon, R. A. (2020). Comparative
599 analysis of building insulation material properties and performance. Renewable and
600 Sustainable Energy Reviews, 131(March), 110038.
601 https://doi.org/10.1016/j.rser.2020.110038

602 Çengel, Y.A., & Ghajar, A.J. (2020). Heat and mass transfer: fundamentals and applications.
603 New York, NY.

604 Bourdot, A., Moussa, T., Gacoin, A., Maalouf, C., Vazquez, P., Thomachot-Schneider, C., …
605 Polidori, G. (2017). Characterization of a hemp-based agro-material: Influence of starch ratio
606 and hemp shive size on physical, mechanical, and hygrothermal properties. Energy and
607 Buildings, 153, 501–512. https://doi.org/10.1016/j.enbuild.2017.08.022

608 Mao, D., Grillet, A., My, T., Diep, H., Nhan, C., Thuc, H., & Woloszyn, M. (2017).
609 Hygrothermal properties of bio-insulation building materials based on bamboo fibers and bio-
610 glues. Construction and Building Materials, 155, 852–866.
611 https://doi.org/10.1016/j.conbuildmat.2017.08.075

612 Bakatovich, A., Gaspar, F., & Boltrushevich, N. (2022). Thermal insulation material based on
613 reed and straw fibres bonded with sodium silicate and rosin. Construction and Building
614 Materials, 352(January), 129055. https://doi.org/10.1016/j.conbuildmat.2022.129055

615

616 ## VIII. List of symbols

Symbol	Definition
$Ra_{x,y}$	Thermal resistance of an air space limited by points x and y (m^2.K/W)
$ha_{x,y}$	Heat transfer coefficient by natural convection/conduction between the cold and hot surfaces of an air space limited between points x and y (W/m^2.K)
$hr_{x,y}$	Heat transfer coefficient by radiation between two isothermal parallel surfaces of an air space limited between points x and y (W/m^2.K)
Th $hole_x$	Average isothermal hot temperature of vertical surface limiting air space at point x (K)
Tc $hole_y$	Average isothermal cold temperature of vertical surface limiting air space at point y (K)
dx_y	Air space thickness between points x and y (m)
bx_y	Air space width between points x and y (m)
ε_x	Total hemispherical emissivity of the hot surface at point x limiting air cavity
ε_y	Total hemispherical emissivity of the cold surface at point y limiting air cavity
ρ	Density (kg/m)
Cp	Specific heat capacity (J/kg.K)
λ	Thermal conductivity (W/m.K)
μ	Dynamic viscosity (kg/m.s)
V	Kinematic viscosity (m^2/s)
β	Thermal expansion coefficient (K^{-1})
Pr	Prandtl number
α	Thermal diffusivity (m^2/s)
T1,T2	Average hole surface temperatures (k)
D	Hole diameter (m)
L	Hole equivalent length (m)
Rx,y	Thermal resistance of S/BP brick between points x and y (m^2.K/W)
ex,y	Thickness of S/BP brick limited by points x and y (m)
λm	Thermal conductivity of S/BP bio-composite (W/m.K)
Φ	Heat flux (W)
S	Surface Area (m^2)

Ti	Room Internal temperature (K)
Te	Room external temperature (K)
Rs,i	Inner surface thermal resistance due to convection (m^2.K/W)
Rs,e	External surface thermal resistance due to convection (m^2.K/W)
hi	Convective heat transfer coefficient of the internal hot wall side (W/m^2.K)
he	Convective heat transfer coefficient of the external hot wall side (W/m^2.K)
U	Thermal transmittance (W/m^2.K)
Pe	Electrical power developed by the heating chamber (W)
J	Surface radiosity (W/m^2)
e_b	Blackbody total emissive power (W/m^2)
ρ_d	Surface reflectivity
G	Surface irradiation (W/m^2)
G_m(J)	Mutual surface irradiation (W/m^2)
Gamb	Ambient irradiation (W/m^2)
F_{amb}	Ambient view factor
ε_{amb}	Ambient surface emissivity
n	Transparent media refractive index
σ	Stefan-Boltzmann constant (W/(m^2.K^4))
$q_{r,net}$	Net radiative heat flux density (W/m^2)

617